Available online at www.sciencedirect.com
ScienceDirect
Journal of Solid State Chemistry 179 (2006) 3534–3540
JOURNAL OF SOLID STATE CHEMISTRY
www.elsevier.com/locate/jssc

Synthesis and electrochemical properties of nonstoichiometric $LiAl_xMn_{2-x}O_{4-\delta}$ as cathode materials for rechargeable lithium ion battery

Woosuk Cho, Wonkyung Ra, Junichi Shirakawa, Masanobu Nakayama, Masataka Wakihara*

Department of Applied Chemistry, Tokyo Institute of Technology, Ookayama, Meguro-ku, Tokyo 152-8552, Japan

Received 6 April 2006; received in revised form 13 July 2006; accepted 18 July 2006
Available online 21 July 2006

Abstract

Nonstoichiometric spinel oxides, $LiAl_xMn_{2-x}O_{4-\delta}$ ($x = 0.1, 0.2$), were synthesized under controlled partial pressure of oxygen, and their elecrochemical performances were investigated. As an Al content increases, solubility limit of the oxygen nonstoichiometry, δ, increased, while partial molar enthalpy $\Delta\overline{H}_{O_2}$ of the formation of oxygen nonstoichiometry decreased.

Cycle performance of $LiAl_xMn_{2-x}O_4$ showed significant improvement comparing with that of $LiMn_2O_4$ cathode. However, the decrease of theoretical capacity was accompanied with Al doping. Nonstoichiometric $LiAl_xMn_{2-x}O_{4-\delta}$ showed the increase in capacity with keeping good cycle performances as well as stoichiometric $LiAl_xMn_{2-x}O_4$. Although the introduction of oxygen nonstoichiometry leads to the increase of Mn^{3+} which is known as Jahn–Teller ion, DSC curves for $LiAl_xMn_{2-x}O_{4-\delta}$ showed no exothermic peak due to phase transition arising from Jahn–Teller distortion around room temperature.

Keywords: Spinel; Lithium ion battery; Defect; Jahn–Teller distortion

1. Introduction

Lithium manganese oxide, $LiMn_2O_4$ is one of the most widely researched cathode materials in Li-ion secondary batteries because of their low cost, no toxicity, easy preparation process, and higher voltages than currently commercialized $LiCoO_2$ [1,2]. The spinel $LiMn_2O_4$ belongs to cubic space group $Fd\bar{3}m$ in which lithium ions locate at the tetrahedral 8*a* sites, manganese ions at the octahedral 16*d* site, and oxygen ions at the 32*e* sites forming fcc packing arrangements. However, the capacity fading of $LiMn_2O_4$ upon cycling is one of the characteristics that need to be improved for a wide use. For the better cyclic performance, several research groups have investigated the electrochemical properties of partially metal-substituted spinel oxides $LiM_yMn_{2-y}O_4$ (M = metal ions), and significant improvement was observed [3,4]. Although the exact mechanism on their improvement is still uncertain, several reasons were proposed as follows: (1) reinforcement of the chemical bond between transition metals and oxide ions, (2) prevention of the dissolution of Mn^{3+} ions into the electrolyte, which causes a disproportion reaction of $2Mn^{3+} \rightarrow Mn^{2+} + Mn^{4+}$, and (3) suppression of Jahn–Teller distortion due to Mn^{3+} ions [5,6]. The decrease of Mn^{3+} ions, caused by metal substitution, reduces the capacity despite the improvement of cyclability. On the other hand, introduction of oxygen nonstoichiometry into spinel oxides, or such as $LiMn_2O_{4-\delta}$, accompanies the increase of Mn^{3+}, leading to the increase in the capacity [7–15]. Thus, the combination of metal substitution and oxygen nonstoichiometry for $LiMn_2O_4$ cathodes are expected to show that the spinel oxides have good cyclability without fading the capacity. In this study, we synthesized nonstoichiometric $LiAl_yMn_{2-y}O_{4-\delta}$ and investigated their crystal structure and electrochemical

*Corresponding author. Fax: +1 81 3 5734 2146.
E-mail address: mwakihar@o.cc.titech.ac.jp (M. Wakihara).

0022-4596/$ - see front matter © 2006 Elsevier Inc. All rights reserved.
doi:10.1016/j.jssc.2006.07.023

Table 1
δ for single-phase region of $LiAl_xMn_{2-x}O_{4-\delta}$

$LiAl_{0.1}Mn_{1.9}O_{4-\delta}$	$0 \leqslant \delta \leqslant 0.05$
$LiAl_{0.2}Mn_{1.8}O_{4-\delta}$	$0 \leqslant \delta \leqslant 0.07$

properties in terms of Al substitution and oxygen nonstoichiometry (Table 1).

2. Experimental

2.1. Preparation and characterization

Al substituted manganese oxides, $LiAl_xMn_{2-x}O_4$ ($x = 0.1$, 0.2, 0.3, and 0.4) was obtained by solid-state reaction. Li_2CO_3, $Al(OH)_3$, and Mn_2O_3 were used as starting materials. Mixture of them was heated at 750 °C in air for 72 h with intermitted grindings, and then the product was cooled to 300 °C at the rate of 0.5 min^{-1}. The molar ratio of the metals in the compounds was determined by inductively coupled plasma (ICP) spectroscopy. The samples were dissolved in HCl (35 wt%) solution at 80 °C for 6 h. Because the obtained composition shows good agreement between analytical and nominal compositions within experimental error, nominal compositions will be used in this paper.

Nonstoichiometric $LiAl_xMn_{2-x}O_{4-\delta}$ was gained as the followed procedures: The above product of $LiAl_xMn_{2-x}O_4$ was heated again at 750 °C for 10 h under various partial pressure of oxygen, which was controlled by mixing O_2 and N_2 gases, and then cooled rapidly into the vessel keeping 0 °C with iced water.

In order to estimate the amount of oxygen defect, thermogravimetry (TG) measurement was performed. Stoichiometric $LiAl_xMn_{2-x}O_4$ was placed in platinum holder, then heated at 750 °C under controlled partial pressure of oxygen, Po_2. Al_2O_3 was used as a reference material. The weight loss arising from formation of oxygen nonstoichiometry was measured after reaching equilibrium state, and the amount of oxygen nonstoichiometry, δ for $LiAl_xMn_{2-x}O_{4-\delta}$ was calculated from these weight losses. At isotherm condition, the measured weight of spinel samples decreased gradually with reducing partial pressure of oxygen under lower P_{O_2} region. On the other hand, no marked change in sample weight was observed under higher P_{O_2} region ($P_{O_2} \geqslant 10^{-0.8}$ and $10^{-0.6}$ atm for $x = 0.1$ and 0.2, respectively). Therefore, we assigned the composition of spinels at higher P_{O_2} region as stoichiometric spinel of $LiAl_xMn_{2-x}O_4$ ($\delta = 0$) for the convenience, hereunder (in the present study, the δ was set as 0 using the weight of sample at $\log P_{O_2} = 0$ atm (750 °C). The exact stoichiometry is yet uncertain, and details are discussed later. TG measurement was also carried out under isothermal condition at 750 °C for estimating the partial molar entropy of the formation of oxygen deficiency.

Phase identification was carried out by X-ray diffraction (XRD) using Cu$K\alpha$ radiation (RINT-2500V, Rigaku Co. Ltd.) at 50 kV/150 mA over 2θ ranging from 10° to 100°. The lattice parameters were determined by the least-squares method using several diffraction peaks with NIST Si powder as a standard material.

Density measurement was performed by the Archimedes method. The density is calculated from the following equation:

$$d(\mathrm{g\,cm^{-3}}) = d_{\mathrm{liquid}} w_2/(w_1 + w_2 - w_3), \quad (1)$$

where w_1 is the weight of liquid filled in the pycnometer, w_2 is the weight of sample, w_3 is the weight of both sample and liquid filled in the pycnometer and d_{liquid} the density of liquid. Toluene (Wako Pure Chemical Industries, 99.8%) was used as liquid.

In order to investigate the thermal structural property of stoichiometric $LiAl_xMn_{2-x}O_4$ and nonstoichiometric $LiAl_xMn_{2-x}O_{4-\delta}$, differential scanning calorimetric (DSC) analysis was performed in the temperature range from 340 to 200 K with cooling rate of 10 K min^{-1}. The samples, $LiMn_2O_4$, $LiAl_xMn_{2-x}O_4$ and $LiAl_xMn_{2-x}O_{4-\delta}$, of 10 mg were sealed into aluminum pan and then set in the measuring apparatus (DSC 6200, Seiko Instruments). The measurements were performed under N_2 gas atmosphere.

2.2. Electrochemical properties

Coin-type cell (CR2032) was utilized to perform electrochemical measurement. Slurry of 80 wt% of spinel material, 10 wt% of acetylene black (conductive agent), and 10 wt% of polyvinylidene fluoride (PVdF) was ground along with *n*-metyl-2-pyrolidinone (NMP) and coated on an Al-foil. A disk of Al-foil was cut off as the cathode. Al-foil diameter was 16 mm and effective material area was 1 cm^2 with 1–1.5 mg. The coin cell was composed of the above cathode disk, lithium metal as the anode, and 1 M $LiClO_4$ solved in ethylene carbonate (EC) and diethyl carbonate (DEC) (1:1 in volume ratio) as the electrolyte (Tomiyama Pure Chemical Ind. Co. Ltd.). All cells were assembled in a glove box filled with Ar gas to avoid any possible air caused side-reaction at ambient temperature.

The cell was charged and discharged at a constant current of 0.2 mA cm^{-2} at room temperature with the cut-off voltage between 3.5 and 4.3 V.

3. Results and discussions

3.1. Structural identification and thermal property

The powder X-ray diffraction patterns for $LiAl_xMn_{2-x}O_4$ ($x = 0$, 0.1, 0.2, 0.3, and 0.4) are shown in Fig. 1. XRD patterns of $LiAl_xMn_{2-x}O_4$ indicate that Al amount up to 0.2 were single phase with cubic symmetry and space group $Fd\bar{3}m$, while impurity peaks were observed around $x = 0.3$ and 0.4.

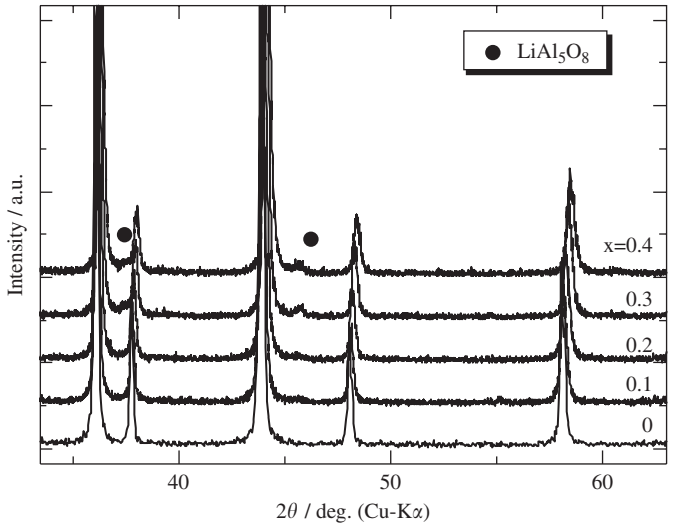

Fig. 1. XRD patterns of $LiAl_xMn_{2-x}O_4$.

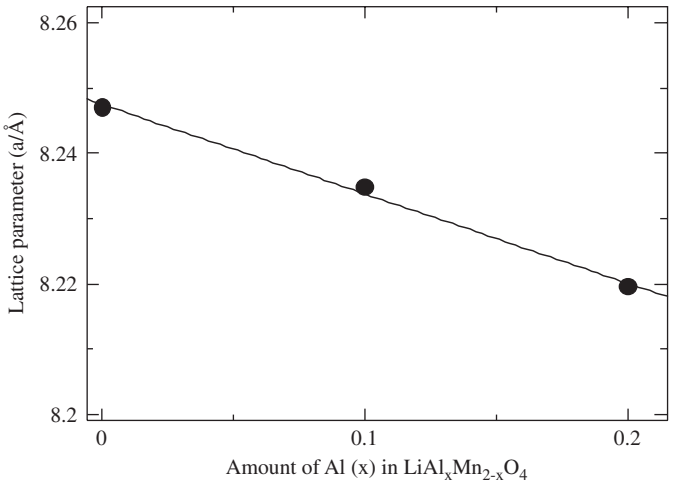

Fig. 2. Lattice parameters of $LiAl_xMn_{2-x}O_4$.

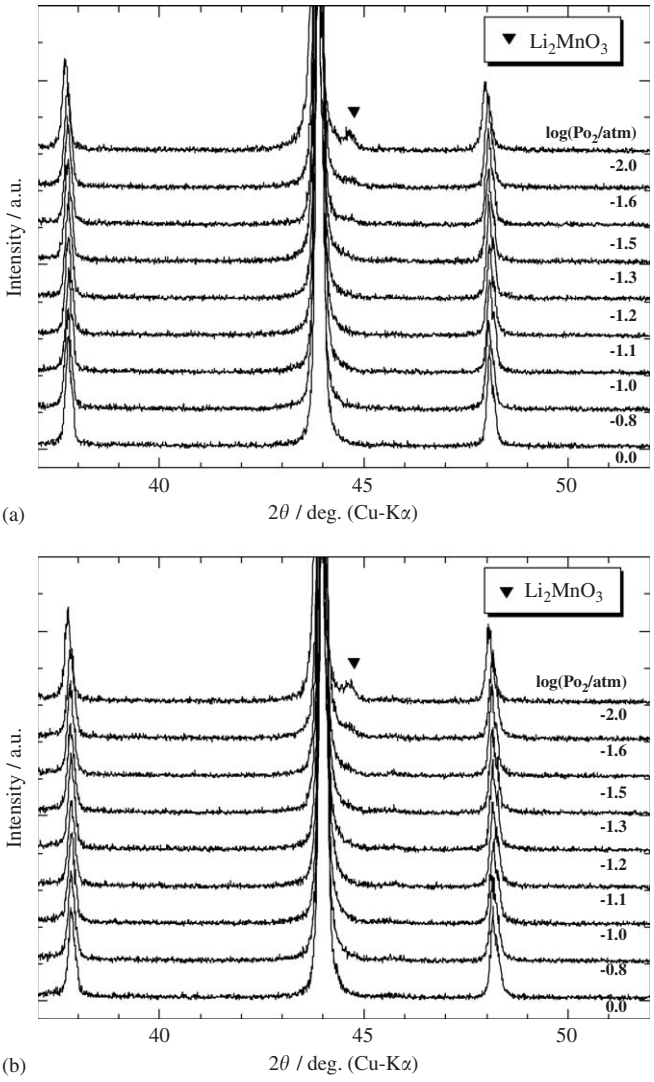

Fig. 3. Variation of the XRD patterns with partial oxygen pressure, $\log P_{O_2}$, for (a) $LiAl_{0.1}Mn_{1.9}O_{4-\delta}$, (b) $LiAl_{0.2}Mn_{1.8}O_{4-\delta}$. Reverse solid triangle indicates impurity phase of Li_2MnO_3.

The lattice parameters of $LiAl_xMn_{2-x}O_4$ (Fig. 2), which are obtained in single-phase region, decrease monotonically with aluminum content. The decrease in lattice parameter can be explained by the fact that ionic radii of aluminum is smaller than that of manganese (0.79 Å for Mn^{3+}, 0.39 Å for Al^{3+}) [16]. Therefore, it was confirmed that the aluminum ions replaced the manganese ions keeping spinel structure.

Fig. 3 shows XRD patterns of nonstoichiometric $LiAl_xMn_{2-x}O_{4-\delta}$ ($x = 0.1, 0.2$). The single-phase regions of $LiAl_xMn_{2-x}O_{4-\delta}$ with partial pressure of oxygen were determined according to the pattern of XRD. An impurity peak of monoclinic Li_2MnO_3 was detected at around $2\theta = 44.66^\circ$ under small P_{O_2} condition, and the peak intensity increased with increasing oxygen defect amount, δ. Reducing the oxygen pressure would lead to the decomposition reaction of $LiMn_2O_{4-\delta}$ as below [17]:

$$2LiMn_2O_{4-\delta} \rightarrow Li_2MnO_3 + Mn_3O_4 + (1-2\delta)/2O_2.$$

Therefore, the single phase of nonstoichiometric spinel could be synthesized under the condition of $\log P_{O_2} \geqslant -1.4$ atm ($x = 0.1$) and -1.3 atm ($x = 0.2$), respectively. The amount of oxygen defect δ for $LiAl_xMn_{2-x}O_{4-\delta}$ was estimated from the results of TG measurement as mentioned in the experimental section. Thus, the single-phase region in present synthesis condition was determined as follows; $0 \leqslant \delta \leqslant \sim 0.05$ for $LiAl_{0.1}Mn_{1.9}O_{4-\delta}$ and $0 \leqslant \delta \leqslant \sim 0.07$ for $LiAl_{0.2}Mn_{1.8}O_{4-\delta}$, respectively.

We investigated the relationship between the lattice parameter of $LiAl_xMn_{2-x}O_{4-\delta}$ ($x = 0.1$ and 0.2) as a function of oxygen nonstoichiometry, δ in Fig. 4. Lattice parameters increased proportionally with increasing δ. This is attributed to the increase of larger Mn^{3+} ions [18], since oxygen defect caused the reduction of Mn^{4+} into Mn^{3+}. In addition, interstitial metals would contribute to the expansion of the cell according to the defect structure as mentioned below. (The density measurement indicated no

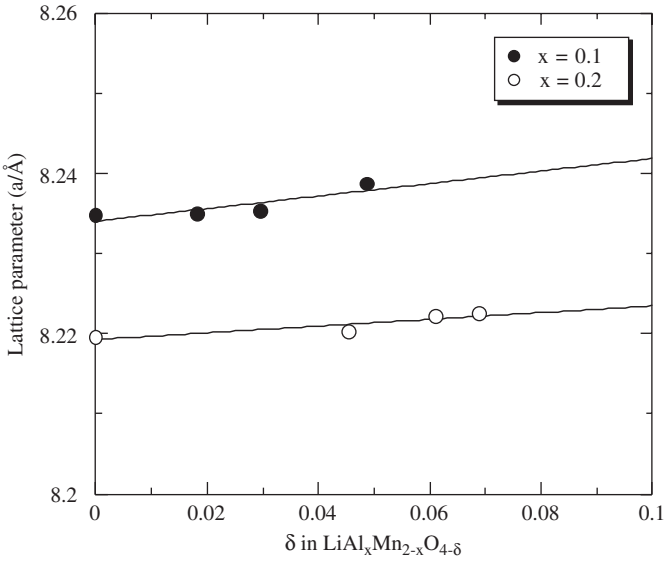

Fig. 4. Lattice parameters of $LiAl_xMn_{2-x}O_{4-\delta}$.

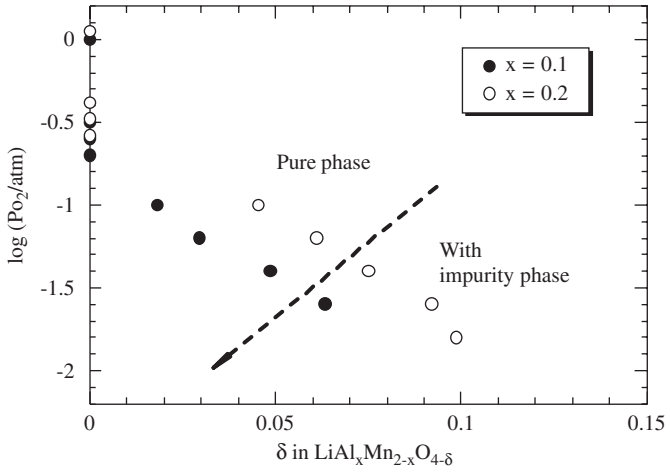

Fig. 5. Amount of oxygen defect δ in $LiAl_xMn_{2-x}O_{4-\delta}$ as a function of $\log P_{O_2}$ at 750 °C. Estimation of δ was made from the data of weight loss. Hatched line implies the defect formation limit boundary which was confirmed by XRD. (Impurity phase of $LiMn_2O_3$ was detected beyond boundary composition, see text.)

oxygen vacancies but interstitial metals reside in $LiAl_xMn_{2-x}O_{4-\delta}$.)

Fig. 5 represented the relationship between oxygen nonstoichiometry δ and partial pressure of oxygen, $\log P_{O_2}$ at 750 °C. The results showed that weight losses increased almost linearly with the decrease of $\log P_{O_2}$. In addition, the amount of δ is larger in $LiAl_{0.2}Mn_{1.8}O_4$ than that observed in $LiAl_{0.1}Mn_{1.9}O_4$ at the same P_{O_2}. The thermodynamic functions of the formation of the oxygen nonstoichiometry in $LiMn_2O_{4-\delta}$ has been reported by Sugiyama et al. [19,20]. The partial molar enthalpy $\Delta\overline{H}_{O_2}$ of the formation of oxygen deficiency are given by

$$\Delta\overline{G}_{O_2} = RT \ln P_{O_2} = \Delta\overline{H}_{O_2} - T\Delta\overline{S}_{O_2}, \quad (2)$$

where, $\Delta\overline{G}_{O_2}$ is the partial molar free energy, R is the gas constant and T is the absolute temperature. Therefore $\Delta\overline{H}_{O_2}$ can be expressed as follows:

$$\Delta\overline{H}_{O_2} = \left[\frac{\partial(R \ln P_{O_2})}{\partial(1/T)}\right]_{\delta}. \quad (3)$$

In other words, $\Delta\overline{H}_{O_2}$ can be obtained by plotting $\log P_{O_2}$ as a function of reciprocal temperature. Fig. 6(a) shows $\log P_{O_2}$ versus $1/T$ for $x = 0.1$ and 0.2 at $\delta = 0.045$. Linear relationships were clearly observed, and the sample with $x = 0.2$ shows steeper slope. The values of $\Delta\overline{H}_{O_2}$ were estimated to be -289 and $-311\,kJ\,mol^{-1}$ for $x = 0.1$ and 0.2 by using Eq. (3), respectively, which showed higher enthalpy than that of parent $LiMn_2O_4$ ($-208\,kJ\,mol^{-1}$) reported by Sugiyama et al. [18] (Fig. 6(b)). Accordingly, the formation enthalpy decreased with the increase in the amount of Al doping, suggesting that Al doping lead to increase the amount of defect δ at the same P_{O_2} (Fig. 5).

Two kinds of structural model of oxygen nonstoichiometic spinels has been proposed as follows: (1) oxygen defect model of $(Li)_{8a}[M_yMn_{2-y}]_{16d}[O_{4-\delta}]_{32e}$ ($M = Li^+$, Mn^{3+}, Mn^{4+} and/or Al^{3+}) and (2) metal excess model of

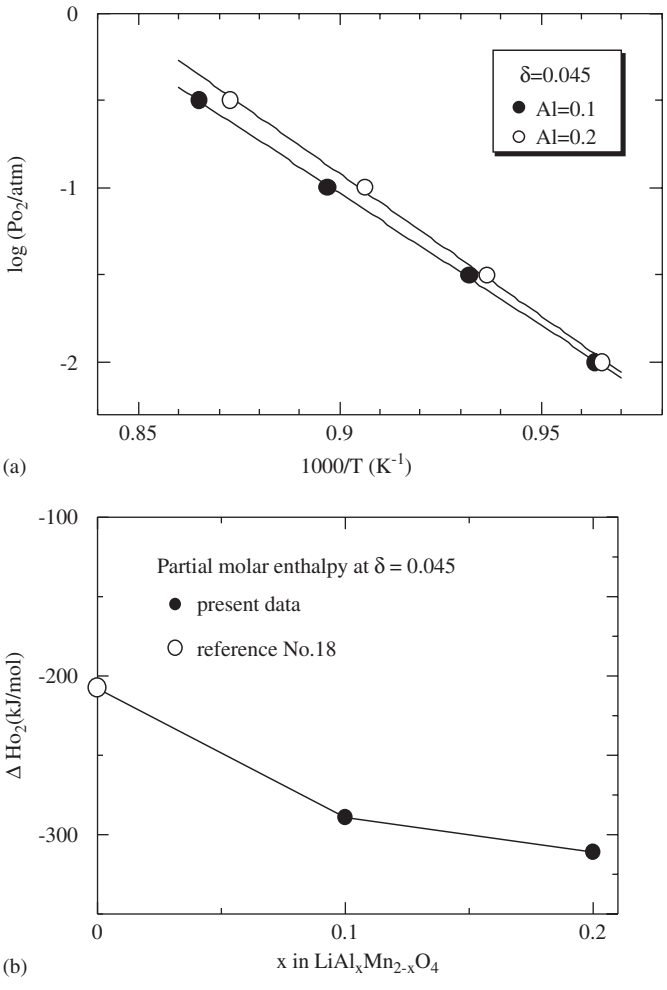

Fig. 6. (a) The dependences of $\log P_{O_2}$ on reciprocal temperature T^{-1}, (b) $\Delta\overline{H}_{O_2}$ for nonstoichiometric $LiAl_xMn_{2-x}O_{4-\delta}$ at $\delta = 0.045$ ($\Delta\overline{H}_{O_2}$ of $LiMn_2O_4$ is from Ref. [18]).

$(Li)_{8a}[Li_{\delta/(4-\delta)}Mn_{2\delta/(4-\delta)}]_{16c}[Mn_2]_{16d}[O_4]_{32e}$.[14,18,21]. For oxygen deficiency model, oxygen site (32*e*) exists as vacancy. Consequently, the theoretical density of the oxygen deficiency model is decreased with the increase of δ. Whereas excess Li, Al and/or Mn occupy vacant 16*c* sites for metal excess model. Therefore, the theoretical density of the metal excess model increases with increasing δ. To clarify which model can be applied to nonstoichiometric $LiAl_xMn_{2-x}O_{4-\delta}$, density measurement was performed (Fig. 7). The observed density of nonstoichiometric $LiAl_xMn_{2-x}O_{4-\delta}$ increased with increasing δ and showed our nonstoichiometric compounds be explained by the metal-excess model. This result suggests that excessive cations (Li^+, Mn^{3+}, Mn^{4+} and/or Al^{3+}) might reside in the empty 16*c* sites, and agrees with the previous report for $LiMn_2O_{4-\delta}$ and $LiMg_yMn_{2-y}O_{4-\delta}$ system [18,21].

3.2. Electrochemical properties

Fig. 8 illustrates the profiles of the first discharge curves at the rate of 0.1 °C for stoichiometric $LiAl_xMn_{2-x}O_4$

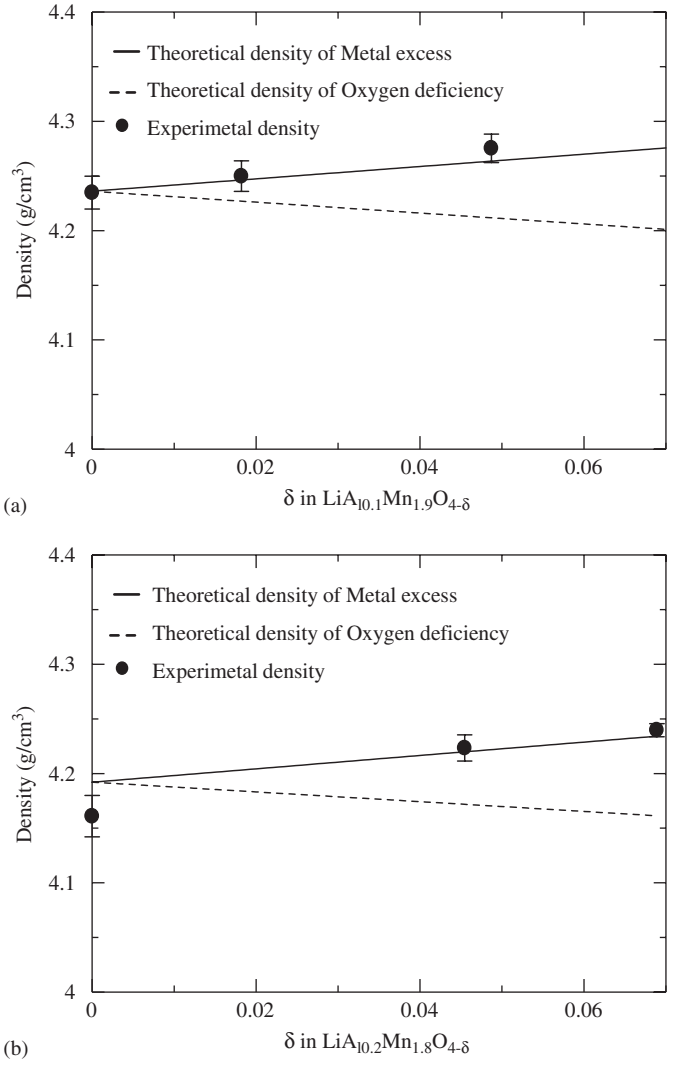

Fig. 7. Densities of (a) $LiAl_{0.1}Mn_{1.9}O_{4-\delta}$ and (b) $LiAl_{0.2}Mn_{1.8}O_{4-\delta}$.

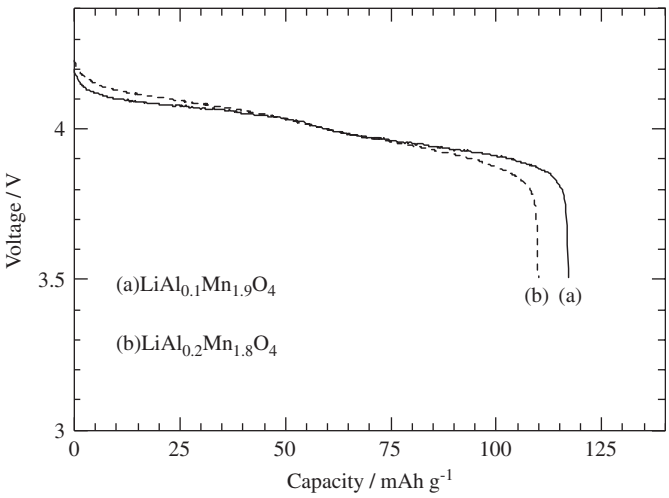

Fig. 8. First discharge curves for stoichiometric $LiAl_xMn_{2-x}O_4$.

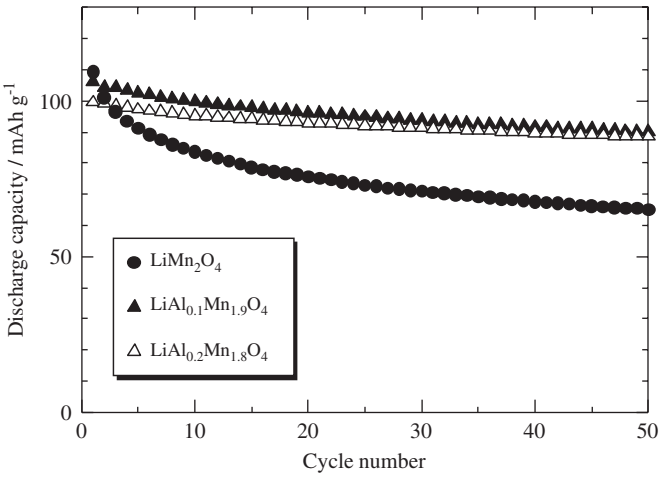

Fig. 9. Cycle performance for stoichiometric $LiAl_xMn_{2-x}O_4$.

($x = 0.1,\ 0.2$). The sample with $x = 0.1$ shows larger capacity than $x = 0.2$. This is due to the decrease of Mn^{3+} ions with Al doping, where Mn^{3+} oxidize to Mn^{4+} during charging. In other words, initial amount of Mn^{3+} ions regulates the total capacity of charging and discharging around 4 V region so that less capacity was expected by larger Al substitution. Fig. 9 shows cycle performance for $LiMn_2O_4$ and Al-doped $LiAl_xMn_{2-x}O_4$. Al-substitution brings out good cyclability, with $LiAl_{0.2}Mn_{1.8}O_4$ showing better cycle performance than $LiAl_{0.1}Mn_{1.9}O_4$.

Improvement of cycle performance is manifested by Al doping, even though doping leads to initial capacity loss resulting from the decrease of redox species of Mn^{3+}. As described in the introduction section, the improvement of cycle performance could be deeply related to the decrease of Mn^{3+}, the electronic configuration ($t_{2g}^3e_g^1$) of which causes cooperative Jahn–Teller phase transition, or Mn^{3+} ion dissolution into electrolyte solution due to dispropotion reaction. In other words, the only alternative to poor cycle performance is to reduce theoretical capacity by

reducing Mn^{3+} content in spinel $LiMn_2O_4$-related electrodes. For example, Yamada et al. reported that the occurrence of the cooperative Jahn–Teller distortion, which is one of the conceivable reason for capacity fading, deeply relate to the concentration of Mn^{3+} in the spinel structure [22].

Fig. 10 show first discharge curves for stoichiometric spinel and nonstoichiometric spinel with maximum value of oxygen nonstoichiometry δ. The capacities of nonstoichiometric spinel were larger than that of stoichiometric one. Capacities of $LiAl_{0.1}Mn_{1.9}O_{4-\delta}$ ($\delta = 0$ and 0.05) were 116 and 125 mAh g^{-1}, respectively. And, capacities of $LiAl_{0.2}Mn_{1.8}O_{4-\delta}$ ($\delta = 0$ and 0.07) were 110 and 116 mAh g^{-1}, respectively. The increase of capacity stems from the increase of Mn^{3+}, which caused by the charge compensation of defect creation [23]. However, the increase of Mn^{3+} is considered to cause poor cyclability as mentioned above.

Fig. 11 presents the cyclability of nonstoichiometric $LiAl_xMn_{2-x}O_{4-\delta}$. Despite the increase of Mn^{3+} concentration (as large as original $LiMn_2O_4$), no marked capacity fading was observed. Furthermore, nonstoichiometric $LiAl_xMn_{2-x}O_{4-\delta}$ show higher capacities than stoichiometric $LiAl_xMn_{2-x}O_4$ during cycles. Accordingly, introduction of both the Al doping and oxygen nonstioichiometry in $LiMn_2O_4$ can improve the cycle performance without reducing the initial capacity. And the cycle performance of $LiMn_2O_4$-related materials does not depend only on the Mn^{3+} contents, but also other factors, such as chemical bond of Al–O and/or defect structure. In this viewpoint, one can assume that Jahn–Teller effect is suppressed even though the Mn^{3+} ion is increased on $LiAl_xMn_{2-x}O_{4-\delta}$. To clarify the effect of Jahn–Teller distortion, DSC measurement was performed. For $LiMn_2O_4$, exothermic peak due to the phase transition of Jahn–Teller distortion was clearly observed at around 280 K in the DSC curves measured on cooling process, which shows good accordance with previous research [22]. By contrast, no Jahn–Teller peaks were appeared for Al substituted stoichiometric $LiAl_xMn_{2-x}O_4$ and even for nonstoichiometric $LiAl_xMn_{2-x}O_{4-\delta}$ as shown in Fig. 12. Therefore the cooperative Jahn–Teller distortion was suppressed for oxygen defect introduced $LiAl_xMn_{2-x}O_{4-\delta}$, even though the amount of Mn^{3+} ions are as large as original $LiMn_2O_4$. Rodríguez-Carvajal et al. proposed that

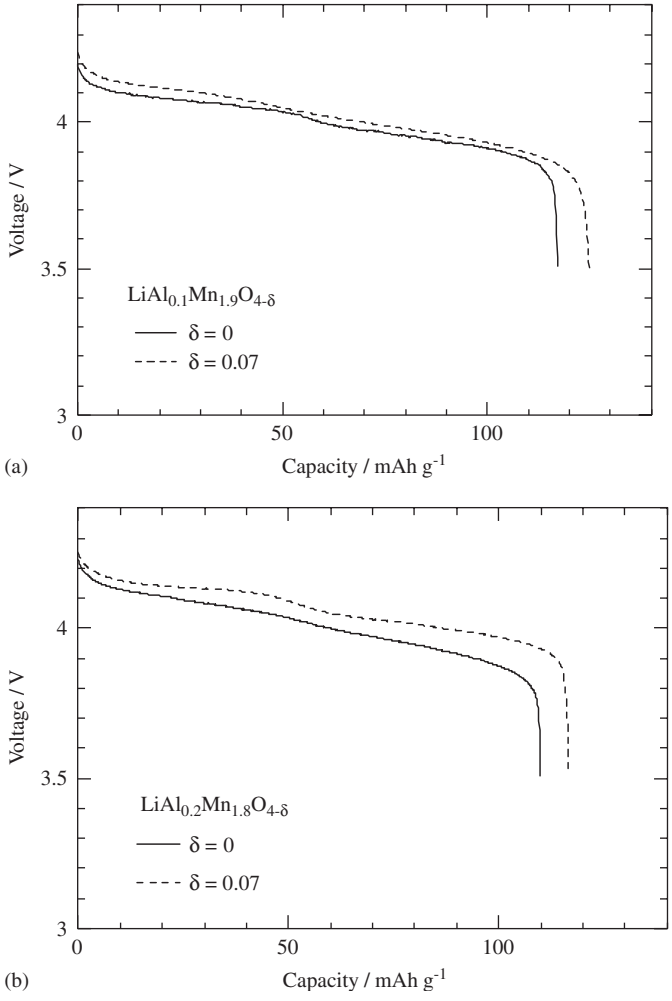

Fig. 10. First discharge curves for nonstoichiometric $LiAl_xMn_{2-x}O_{4-\delta}$.

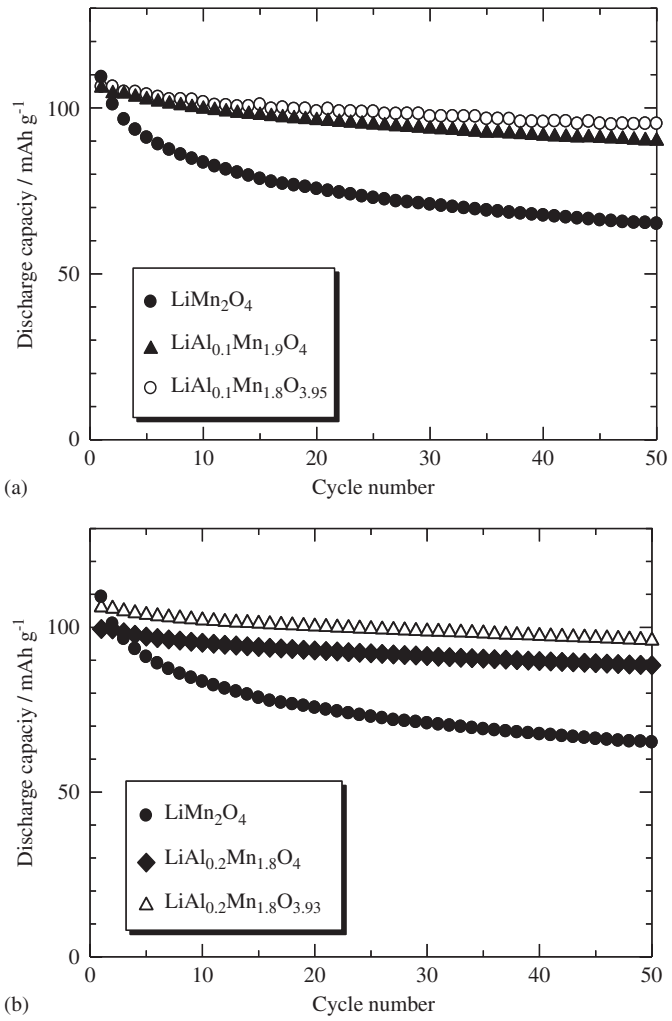

Fig. 11. Cycle performance for nonstoichiometric $LiAl_xMn_{2-x}O_{4-\delta}$.

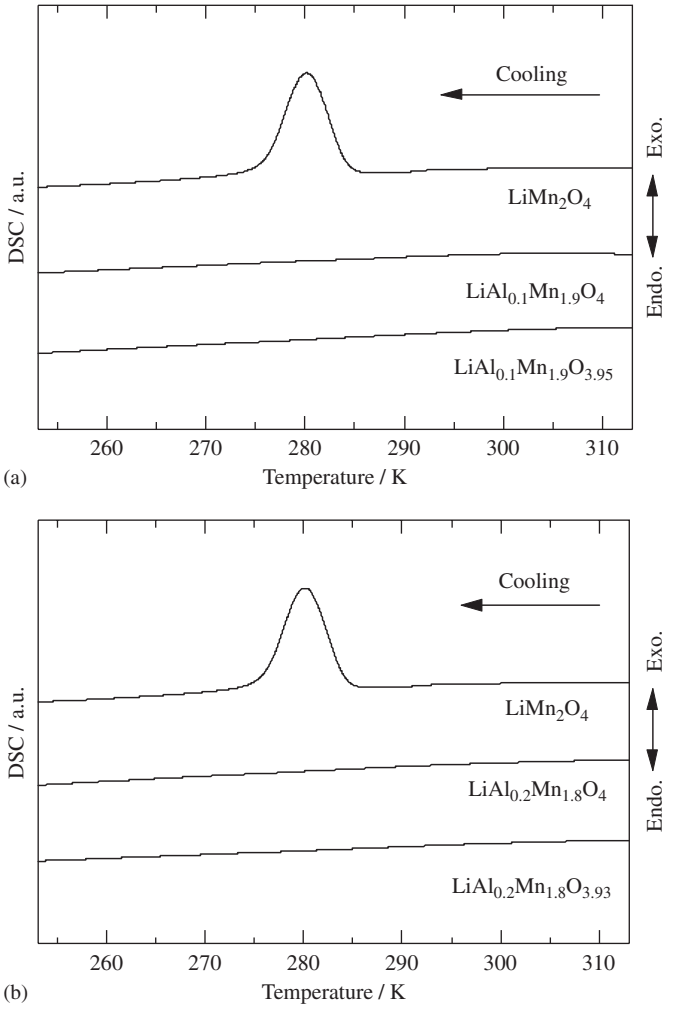

Fig. 12. DSC curves for nonstoichiometric (a) $LiAl_{0.1}Mn_{1.9}O_{4-\delta}$ and (b) $LiAl_{0.2}Mn_{1.8}O_{4-\delta}$.

the Jahn–Teller effect was accompanied with charge ordering of Mn^{3+}/Mn^{4+} simultaneously in the structure [24]. Thus, it proposed in this study that Al substitution and oxygen nonstoichiometry (which leads to occupation of portion of metals at the vacant 16*c* sites) prevents the ordered arrangement of Mn^{3+}/Mn^{4+}. This leads to the suppression of Jahn–Teller distortion according to Rodríguez-Carvajal et al. [24]. Accordingly, the improvement of cycle performance is achieved despite the increase of Mn^{3+} contents by introducing oxygen nonstoichiometry, δ.

Therefore oxygen defect introduced $LiAl_xMn_{2-x}O_{4-\delta}$ would be an attractive cathode material, since poor cycle performance was improved by Al-substitution and capacity was increased through the introduction of oxygen defect. Finally, the introduction of oxygen defect seems to suppress overpotential as shown in Fig. 10. Existence of interstitial metals may negatively affect Li diffusion. However, the total amount of interstitial metals are small, and positive effect of the lattice expansion would support lithium diffusion. Additional investigations are required for further discussion concerning this matter.

4. Conclusion

Synthesis and electrochemical properties of nonstoichiometric $LiAl_xMn_{2-x}O_{4-\delta}$ as cathode material on Li-ion secondary battery were investigated in this study. Relationship between amount of doped Al and oxygen defect was investigated as a function of temperature and partial pressure of oxygen. Accordingly, the partial molar enthalpy $\Delta\overline{H}_{O_2}$ of the formation of oxygen deficiency decreased with the increase in the amount of Al doping, and it leads to increase the amount of defect δ at the same P_{O_2}. Nonstoichiometric $LiAl_xMn_{2-x}O_{4-\delta}$ showed good cycle performance with keeping capacity as large as parent $LiMn_2O_4$, which were induced by substitution of Al and introduction of oxygen nonstoichiometry. It is assumed that suppression of the phase transition due to Jahn–Teller distortion improves the electrochemical performance, which is proved by DSC measurement, even though the Mn^{3+} content increases.

References

[1] Y. Nishi, J. Power Sources 100 (2001) 101.
[2] M. Wakihara, Mater. Sci. Eng. Res. 33 (2001) 109.
[3] G. Li, H. Ikuta, T. Uchida, M. Wakihara, J. Electrochem. Soc. 143 (1996) 178.
[4] R.J. Gummow, A. de Kock, M.M. Thackeray, Solid State Ion. 69 (1994) 59.
[5] G.G. Amatucci, C.N. Schmutzs, A. Blyr, C. Sigala, A.S. Gozdz, D. Larcher, J.M. Tarascon, J. Power Sources 69 (1997) 11.
[6] Y. Xia, M. Yoshio, J. Electrochem. Soc. 143 (1996) 825.
[7] D. Song, H. Ikuta, T. Uchida, M. Wakihara, Solid State Ion. 117 (1999) 151.
[8] H. Kawai, M. Nagata, H. Tukamoto, A.R. West, J. Power Sources 81–82 (1999) 67.
[9] R. Basu, R. Seshadri, J. Mater. Chem. 10 (2000) 507.
[10] J. Sugiyama, T. Atsumi, A. Koiwai, T. Sasaki, T. Hioki, S. Noda, N. Kamegashira, J. Phys.: Condens. Matter 9 (1997) 1729.
[11] J. Molenda, K. Swierczek, J. Marzec, R.C. Liu, Solid State Ion. 157 (2003) 101.
[12] X. Wang, H. Nakamura, M. Yoshio, J. Power Sources 110 (2002) 19.
[13] M. Tachibana, T. Tojo, H. Kawaji, T. Atake, H. Ikuta, Y. Uchimota, M. Wakihara, Phys. Rev. B 66 (2002) 092406.
[14] M. Hosoya, H. Ikuta, M. Wakihara, Solid State Ion. 111 (1998) 153.
[15] Z. Wang, H. Ikuta, Y. Uchimoto, M. Wakihara, J. Electrochem. Soc. 150 (9) (2003) A1250.
[16] R.D. Shannon, Acta Crystallogr. A 32 (1976) 752.
[17] R. Yamaguchi, H. Ikuta, M. Wakihara, J. Therm Anal. Calorim. 57 (1997) 797.
[18] M. Hosoya, H. Ikuta, T. Uchita, M. Wakihara, J. Electrochem. Soc. 144 (4) (1997) L52.
[19] J. Sugiyama, T. Atsumi, T. Hioki, S. Noda, N. Kamegashira, J. Allows Compounds 235 (1996) 163.
[20] J. Sugiyama, T. Atsumi, T. Hioki, S. Noda, N. Kamegashira, J. Power Sources 68 (1997) 641.
[21] N. Hayashi, H. Ikuta, M. Wakihara, J. Electrochem. Soc. 146 (1999) 1351.
[22] A. Yamada, M. Tanaka, Mater. Res. Bull. 30 (6) (1995) 715.
[23] T. Ohzuku, M. Kitagawa, T. Hirai, J. Electrochem. Soc. 137 (1990) 769.
[24] J. Rodríguez-Carvajal, G. Rousse, C. Masquelier, M. Hervieu, Phys. Rev. Lett. 81 (1998) 4660.